https://doi.org/10.5194/egusphere-2022-1308
Preprint. Discussion started: 9 January 2023
© Author(s) 2023. CC BY 4.0 License.

"Human displacements from tropical cyclone Idai attributable to climate change"

Benedikt Mester [1, 2], Thomas Vogt [1], Seth Bryant [2, 3], Christian Otto [1], Katja Frieler [1], and Jacob Schewe [1]

[1] Potsdam Institute for Climate Impact Research, Potsdam, Germany
[2] Institute of Environmental Science and Geography, University of Potsdam, Potsdam, Germany
[3] GFZ German Research Centre for Geosciences, Potsdam, Germany

Correspondence: Benedikt Mester (benedikt.mester@pik-potsdam.de)

Abstract

Extreme weather events often trigger massive population displacement. A compounding factor is that the frequency and intensity of such events is affected by anthropogenic climate change. However, the effect of historical climate change on displacement risk has so far not been quantified. Here, we show how displacement can be partially attributed to climate change, using the example of the 2019 tropical cyclone Idai in Mozambique. We estimate the population exposed to flooding following Idai's landfall, using a combination of storm surge modeling and flood depth estimation from remote sensing images, for factual (climate change) and counterfactual (no climate change) mean sea level and maximum wind speed conditions. We find that climate change has increased displacement risk from this event by approximately 3.1 to 3.5%, corresponding to 16,000 - 17,000 additional displaced persons. Besides highlighting the significant effects on humanitarian conditions already imparted by climate change, our study provides a blueprint for event-based displacement attribution.

1 Introduction

Tropical cyclones (TCs) pose immense risks to coastal communities around the world. Between 1980 and 2021, an average of 45 TCs globally have been recorded per year, with the Philippines, China, Vietnam, USA and Mexico as the top-five most frequently exposed countries (Guha-Sapir et al., 2022). While related monetary losses are high due to the massive damages to housing and infrastructure, TCs also displace an average of 9.3 million people every year, with this hazard being responsible for 43% of all weather-related displacements (IDMC, 2022). Such forced displacements are associated with extensive human suffering, as well as substantial costs (e.g., for providing shelter or from loss of economic production) and often require international assistance for disaster relief funds and humanitarian response (Desai et al., 2021).

At the same time, global climate change is expected to alter TC characteristics, resulting in an increase in overall TC intensity (maximum wind speed and precipitation) and hence in the

https://doi.org/10.5194/egusphere-2022-1308
Preprint. Discussion started: 9 January 2023
© Author(s) 2023. CC BY 4.0 License.

frequency of very intense TCs (category 4-5 on the Saffir-Simpson scale), fundamentally because of an increase in potential intensity due to warmer sea surface temperatures (SST) (Emanuel, 1987; Knutson et al., 2020). Rising sea levels, also driven by global warming, additionally compound coastal flood risk associated with TCs (e.g., Garner Andra J. et al., 2017; Lin et al., 2012; Resio and Irish, 2016). Given that global mean surface air temperature and sea level have already risen substantially above pre-industrial conditions (by about 1.1°C and 0.20 m, respectively (Gulev et al., 2021)), it is likely that recent TC landfalls have caused more severe impacts than would be expected without climate change. However, the portion of TC-induced human displacements attributable to climate change has so far not been quantified.

In this study, we address this research gap for the particular case of displacement triggered by TC Idai in 2019. We examine the floods in central Mozambique associated with TC Idai, considered to be “one of the Southern Hemisphere’s most devastating storms on record” (Warren, 2019). On the 14th of March, Idai made landfall near the densely populated port city of Beira, inhabited by more than 530,000 people (Figure 1). Alongside strong winds and extensive inland flooding caused by heavy rainfall, the cyclone also created an intense storm surge, leading to severe coastal flooding. In Mozambique alone, TC Idai claimed the lives of more than 600 people, and caused 478,000 internal displacements, as well as widespread structural damage totaling more than US$ 2.1 billion (Guha-Sapir et al., 2022; IDMC, 2022).

Here, we investigate how the coastal flooding would have manifested in a counterfactual world without climate change, and consequently, how many of the observed human displacements from TC Idai can be linked to climate change. For the attribution of the impacts we follow the storyline approach introduced by Shepherd (Shepherd, 2016). To this end, we account for two known mechanisms through which global climate change could have affected coastal flood hazard: sea-level rise and amplification of storm intensity. We first estimate the influence of climate change on sea level and TC intensity in the South Indian Ocean. We employ a high-resolution hydrodynamic flood model to simulate TC Idai’s peak coastal flood extent and depth, both under historical conditions and under counterfactual conditions with lower sea levels and lower maximum wind speed, corresponding to a world without climate change. We additionally use satellite imagery to account for inland (freshwater) flooding, and estimate the total number of people affected by flooding. We then model the number of displacements based on flood depth-specific vulnerability factors, and estimate the fraction of displacements that can be attributed to climate change by comparing results under factual vs. counterfactual conditions.

We use an estimate of sea level rise (SLR) that attempts to separate natural variability in ice sheet and glacier mass balance and retain only the long-term trend induced by global warming (Strauss et al., 2021). Beyond this, however, our analysis is indifferent to whether the trends in sea level and TC intensity are anthropogenic or not. This is in line with the definition of *impact attribution* put forward by the Intergovernmental Panel on Climate Change (IPCC), where “changes in natural, human, or managed systems are attributed to [a] change in [a] climate-related system” (O’Neill et al., 2022). Such a question can be separated from the *climate attribution* question of whether the change in the climate-related system - here, sea level and TCs - is due to anthropogenic forcing. This separation allows us to focus on the link between climate change and displacement despite remaining uncertainty about the exact anthropogenic contribution. We will return to this issue below.

https://doi.org/10.5194/egusphere-2022-1308
Preprint. Discussion started: 9 January 2023
© Author(s) 2023. CC BY 4.0 License.

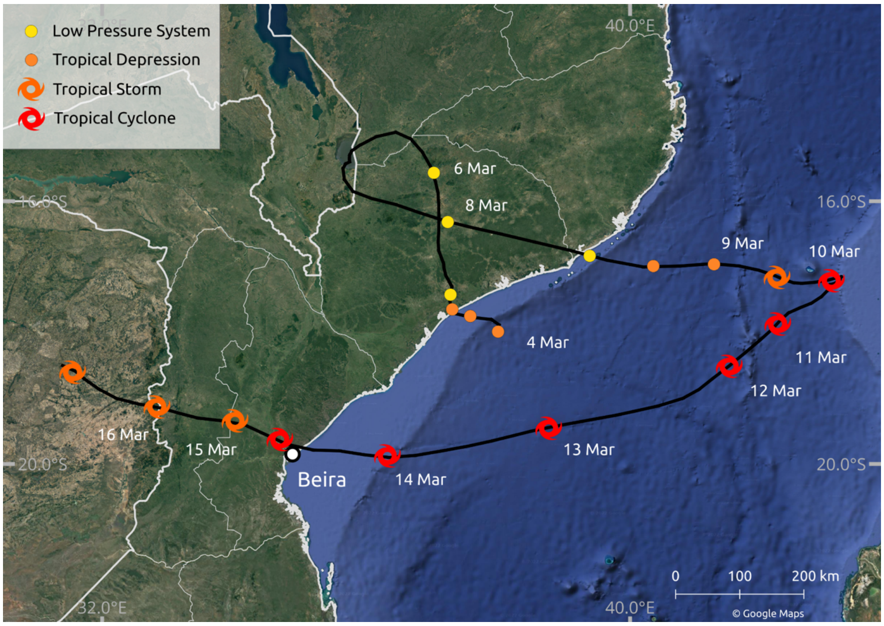

Figure 1: Trajectory of tropical cyclone Idai over the South Indian Ocean. Trajectory data is based on the IBTrACS database (Knapp et al., 2010). Mozambican administrative boundaries (GADM, 2018) in white; satellite image background by © Google Maps (Google Maps (a), 2022). Dates and tropical cyclone status adopted from Reliefweb (Reliefweb, 2019).

2 Methods

2.1 Coastal Flood Modeling

The storm surge flood simulations are generated using the open-source geophysical flow solver GeoClaw (Mandli and Dawson, 2014). GeoClaw uses an efficient adaptive mesh refinement to model wind- and pressure-induced wave dynamics in the 2-dimensional depth-averaged shallow water equations. The detailed model setup used here is described and evaluated by Vogt and colleagues (Vogt et al., 2022).

As the factual input for GeoClaw, the TC track data from IBTrACS (Knapp et al., 2010) provided by the WMO Regional Specialised Meteorological Center at La Reunion (operated by MeteoFrance) is used. For the counterfactual scenarios with modified TC intensity, we multiplied all wind speed values along the track by a scalar factor of 0.9 (for a decrease of 10% in intensity). The central pressure at each track position is increased by 0.1 times the difference between central pressure and environmental pressure.

From the wind speed, pressure, and radius information provided along the TC track, GeoClaw derives surface wind speeds and air pressure at arbitrary locations in space and time using a

https://doi.org/10.5194/egusphere-2022-1308
Preprint. Discussion started: 9 January 2023
© Author(s) 2023. CC BY 4.0 License.

radially symmetric wind profile (Holland, 1980) combined with the influence from the storm's translational speed.

GeoClaw does not incorporate any tidal dynamics, nor meteorological forcings apart from the TC wind and pressure fields mentioned above. To account for the influence of astronomical tides, we configured GeoClaw to use an initial sea level according to gridded satellite altimetry for 2019 (CMEMS, 2021), optionally enhanced by the minimum, mean, or maximum simulated astronomical tides in the region of landfall according to the FES2014 global ocean tide atlas (Lyard et al., 2021). For the counterfactual sea level scenarios, the amount of sea level rise specified in the scenario description (between 6.5 and 17.0 cm) was subtracted from the initial sea level.

The topographical input for GeoClaw is taken from digital elevation models. We used a combination of CoastalDEM 2.1 (Kulp and Strauss, 2021, 2018) in coastal areas, SRTM 15+ V2.3 (Tozer et al., 2019) over the open ocean and Multi-Error-Removed Improved-Terrain (MERIT) digital elevation model (DEM) (Yamazaki et al., 2019) everywhere else. All datasets are converted to the same geoidal vertical datum (EGM96) at a spatial resolution of 9 arcseconds (approximately 300 m).

Due to a lack of tide gauges in Mozambique, it was not possible to validate the performance of GeoClaw for TC Idai in the factual model runs. However, we compared the water levels at a virtual tide gauge station off the coast of Beira, where the highest impacts from TC Idai have been reported, with simulated water levels from the Global Tide and Surge Model (GTSM) (Dullaart et al., 2021; Muis et al., 2020), and found the best agreement of maximum surge heights for the GeoClaw run with the maximum astronomical tide assumption, closely followed by the run with no tidal adjustment (Supplementary Figure S1).

2.2 Inland Flood Depth Estimation

Gridded depth maximums for the flood event (Supplementary Figure S2) were calculated using the Rolling HAND Inundation Corrected Depth Estimator (RICorDE) algorithm (Bryant et al., 2022) supplied with terrain data from the MERIT DEM project, permanent surface water data from the Joint Research Centre (JRC) Global Surface Water project (Pekel et al., 2016), and flood extents from the FloodScan product (Atmospheric and Environmental Research & African Risk Capacity, 2022). MERIT DEM provides a roughly 90 m resolution global layer derived from multiple space-based sensors to minimize elevation errors. The maximum water extent layer from JRC's Global Surface Water project provides a roughly 30 m resolution global layer of locations detected as inundated on Landsat imagery (Wulder et al., 2016) from 1984-2019 (Pekel et al., 2016). Observed flood extents for TC Idai were obtained from Atmospheric and Environmental Research & African Risk Capacity's accumulated 2-tier standard flood extent depiction FloodScan product from 2019-03-01 to 2019-03-31, which has the same resolution as the MERIT DEM. Originally developed for applications in Africa, this FloodScan algorithm relies on satellite based low-resolution passive microwave data to estimate inundation areas. The algorithm was designed to minimize false-positives at the expense of small flood sensitivity (Galantowicz and Picton, 2021). All data layers were re-projected to 90 m resolution geodetic coordinates prior to the RICorDE computation.

https://doi.org/10.5194/egusphere-2022-1308
Preprint. Discussion started: 9 January 2023
© Author(s) 2023. CC BY 4.0 License.

RICorDE is an algorithm originally developed for post-event analysis of fluvial flood events in Canada that produces gridded water depth estimates by incorporating Height Above Nearest Drainage (HAND) and cost distancing sub-routines to extrapolate edge values into an inundation region. By using the vertical distance above the permanent water surface computed in the HAND routine, RICorDE pre-filters egregious flood extent predictions and assumes a water surface slope matching the permanent water surface (rather than the flat surface assumed by similar methods). The slower, more complex RICorDE algorithm has been shown to produce more accurate depths maps when compared to faster, more disaster response-focused solutions like the Floodwater Depth Estimation Tool (FwDET) (Bryant et al., 2022; Cohen et al., 2018).

While no data was available to validate the performance of the depths estimate, visual inspection suggests results are less accurate in areas with higher elevation (>20 m), especially where drainageways are of comparable width to the resolution of the JRC water extent layer. These false negatives in the JRC layer propagate as positive bias in the HAND routine, which leads to higher elevation water surface predictions and similar positive bias in the depth values (see white arrow in Figure S3a).

2.3 Combined Flood Depth Product

The inland flood depth estimates from RICorDE are resampled from 3 arcsec to 9 arcsec, using the average resampling method (Rasterio library for Python), to match the resolution of the GeoClaw output. All flood depths are rounded to the nearest decimeter, their outline is cropped to the area of interest, and the final factual flood depth in each grid cell (shown in Figure 3a) is determined as the maximum of both products. This accounts for both potentially partly obscured satellite imagery by clouds and potential underestimation by the numerical model.

$$d_0 = max\ (d_{c,0} \, , d_r) \qquad (1)$$

with d_0 referring to the factual flood depth, and indices c and r referring to the coastal flood model (GeoClaw) and to the remote sensing data translated into flood depth using RICorDE, respectively. To derive the counterfactual flood depth d_{cf}, we subtract the difference between modeled factual and counterfactual coastal flood depths from the combined factual flood depth:

$$d_{cf} = d_0 \; - \; (d_{c,0} \; - \; d_{c,cf}) \qquad (2)$$

2.4 Displacement

We use displacement data from the openly accessible *Global Internal Displacement Database* (IDMC, 2022). No granular information is available on the type of displacement, e.g., long-term displacement or temporary evacuation, nor on the proportion of displacement by hazard type. We assume that people exposed to flood levels greater or equal than 100 cm are affected by the flooding and thus prone to displacement, following previous studies (Custer and

https://doi.org/10.5194/egusphere-2022-1308
Preprint. Discussion started: 9 January 2023
© Author(s) 2023. CC BY 4.0 License.

Nishijima, 2015; Kam et al., 2021). However, we also test the sensitivity of our results to this threshold choice by evaluating alternative water level thresholds of 10 cm and 50 cm.

We first determine the flood extent with depths greater than the selected water level threshold and overlay it with population data to estimate the number of people affected. We use gridded population data from GHS-POP (Schiavina et al., 2019) for the year 2015, on 9 arcsec resolution. Population growth in Mozambique was 1.12 % between 2015 and 2019 (The World Bank, 2022); we hence multiplied all population grid cells with this factor, assuming a spatially equal population growth.

We then calculate the ratio between the number of observed displacements, and the number of affected people from the factual flood estimate. This ratio, which may be thought of as an event-specific displacement vulnerability factor, is different for every tide assumption, reflecting the uncertainty about the actual flood extent and depth. We compute for every impact level threshold *i* and tide assumption *h* a displacement vulnerability factor $v_{i,h}$ by dividing the number of observed displacements D_o by the total number of affected people of the factual scenario $A_{i,h,o}$:

$$v_{i,h} = \frac{D_0}{A_{i,h,0}} \quad (3)$$

Multiplying the specific displacement vulnerabilities with the counterfactual numbers of affected people, we derive the number of people at risk of displacement in a world without climate change. This means that the difference between factual and counterfactual displacement estimates comes only from differences in the flood hazard, while exposure and vulnerability factors are held fixed. We achieve this by multiplying $v_{i,t}$ with the number of affected people of the counterfactuals $A_{i,h,cf}$, and estimate the expected number of displacements for each counterfactual scenario $D_{i,h,cf}$:

$$D_{i,h,cf} = v_{i,h} * A_{i,h,cf} \quad (4)$$

2.5 High Wind Speed-Induced Displacements

Even though disaster reports for TC Idai suggest flooding to be the main driver of displacement, high wind speeds may have locally intensified the impact of TC Idai (Figure S4) and be partially responsible for the observed displacements. We conduct an additional analysis where we assume that people affected by either flooding or wind (or both) were at risk of displacement with an equal vulnerability factor. We use a wind speed threshold of 96 kn (50 m s^{-1}) for population exposure (Geiger et al., 2018), corresponding to the Saffir–Simpson scale classification 3 (major hurricane). The resulting wind field is overlaid with gridded population data to compute the number of affected people, excluding those who are already affected by flooding.

https://doi.org/10.5194/egusphere-2022-1308
Preprint. Discussion started: 9 January 2023
© Author(s) 2023. CC BY 4.0 License.

3 Results

3.1 Counterfactuals

Constructing counterfactuals for sea level and TC intensity requires estimating the effect of historical climate change on these quantities. Total global mean sea level has risen by approximately 23 cm since the turn of the 20th century (Church and White, 2011); at a rate that has increased over time (Dangendorf Sönke et al., 2017). According to the IPCC, it is very likely that the rate of global mean SLR was 1.5 (1.1 to 1.9) mm yr^{-1} between 1902 and 2010, and 3.6 (3.1 to 4.1) mm yr^{-1} between 2006 and 2015 (Gulev et al., 2021). Nonetheless, regional changes in sea level may differ substantially from the global average due to shifting surface winds, the differential expansion of warming ocean water, and the addition of melting ice, which can alter the ocean circulation (Fox-Kemper et al., 2021). Additionally, increases in the amount of water stored on land (due to construction of dams and reservoirs), as well as land subsidence, have also affected total sea level, with their relative effects varying geographically (Church et al., 2004; Strauss et al., 2021).

Long-term in-situ observational records of SLR are scarce in the Indian Ocean (Han et al., 2010), hampering a precise detection of changes in sea level. For example, no active tide gauge stations can be found on the coast of Beira (Beal et al., 2019), with the nearest station located in Inhambane, Mozambique, 448 km south of Beira. However, regional historical SLR rates for Mozambique, derived from satellite imagery or models, are close to global mean estimates. IPCC rates of change in sea surface height (geocentric sea level) derived from satellite altimetry show regional SLR off the coast of Mozambique at around 4.0 mm yr^{-1} for the period 1993–2012 (Church et al., 2013). Climate-induced SLR at the South-Eastern African coastline (1993 - 2015) is estimated at ~3.5 mm yr^{-1} using a coastal-length weighted approach (Nicholls et al., 2021). Reconstructed sea level fields using global tide gauge data suggests global-averaged SLR at 1.8 ± 0.3 mm yr^{-1} over the 1950-2000 period, with regional SLR off the coast of Mozambique at around 1.5 mm yr^{-1} (Church et al., 2004). Han and colleagues (Han et al., 2010) estimate regional Mozambican SLR at approximately 1.2 mm yr^{-1} between 1961-2008.

Given that these regional estimates are close to the global mean estimate by the IPCC, we assume that total SLR near Beira is the same as the global mean, a comparable approach as by Irish and colleagues (Irish et al., 2014). In order to exclude trends induced by natural variability, particularly in sea level contributions from glaciers and ice sheets, we use estimates of global mean sea level rise attributable to anthropogenic climate change for 1900–2012 from Strauss and colleagues (Strauss et al., 2021).Their ensemble estimate is 6.6 to 17.1 cm, which we use to define counterfactual sea level parameters for the coastal flood model. This also implies assuming no substantial local effects of land subsidence and human-induced changes in land water storage through reservoir construction and groundwater extraction that would confound comparison with the global estimates. This is hard to verify, but can be motivated by findings that city subsidence occurs only in a small fraction of the world's coasts (Nicholls et al., 2021).

Tropical cyclones are projected to become more intense with rising temperatures (Knutson et al., 2015), which is in line with the theoretical understanding of the potential intensity theory

https://doi.org/10.5194/egusphere-2022-1308
Preprint. Discussion started: 9 January 2023
© Author(s) 2023. CC BY 4.0 License.

by Emanuel (Emanuel, 1987). Observed TC wind speed data in the South Indian Ocean basin shows that the maximum 10-minute sustained wind speed has been increasing by about 0.3 kn (0.15 m s^{-1}) per year on average, over the period 1973-2019 (Figure 2). Prior to 1973, the rate of increase was likely smaller, though observational data is lacking. We make a conservative assumption corresponding to 50 years of increase at a rate of 0.2 kn (0.1 m s^{-1}) per year, resulting in a total difference in maximum wind speed of approximately 10 kn (5.1 m s^{-1}). For the case of TC Idai with maximum observed 10-minute sustained wind speeds of 105 kn (54 m s^{-1}), this corresponds to a 10% reduction in maximum wind speed by removing climate change, which we adopt as a plausible assumption about a counterfactual TC de-intensification. This is a larger change than when adopting an earlier model-based estimate of 3.7% increase in maximum surface wind speed per 1 °C of sea surface temperature (SST) rise (Knutson and Tuleya, 2008). However, a trend analysis of global satellite data (1982–2009) finds an observed increase in maximum intensity by 1.7 m s^{-1} per decade ($p = 0.06$) in the south Indian Ocean (Kossin et al., 2013), yielding an increase by about 8.5% when extrapolating this rate of change over the 50 years prior to 2019; which is in closer agreement with our analysis.

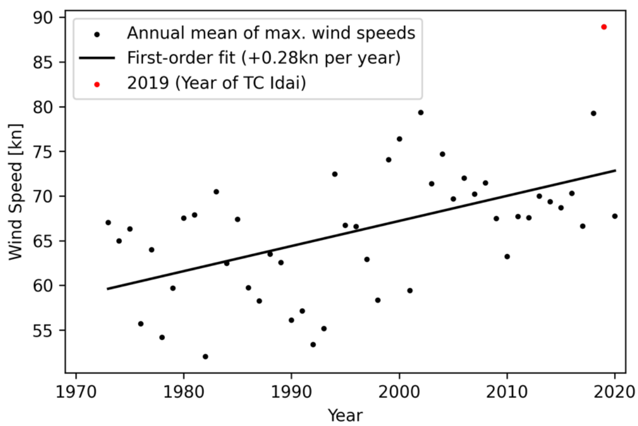

Figure 2: Annual means of maximum TC wind speeds in the South Indian Ocean (maximum 10-minute sustained wind speeds). Linear trend over the period 1973-2020; data from IBTrACS database (Knapp et al., 2010).

3.2 Simulated flooding

We calculate storm surge flood extent and depth for the factual (driven with observed wind speeds and sea levels) and counterfactual (reduced wind speeds and sea level) scenarios, using an open-source geophysical flow solver (see Sect. Methods). The contribution of tides to total sea water levels at the time of landfall is an important yet unknown model parameter. We test four different assumptions about astronomical tide levels, and find that the maximum astronomical tide shows the best agreement with simulated water levels from the Global Tide and Surge Model (Dullaart et al., 2021; Muis et al., 2020), followed by the monthly mean sea level from satellite altimetry without any tidal adjustment (Supplementary Figure S1).

https://doi.org/10.5194/egusphere-2022-1308
Preprint. Discussion started: 9 January 2023
© Author(s) 2023. CC BY 4.0 License.

Both factual and counterfactual coastal flooding are combined with inland flood depth estimates derived from satellite imagery in combination with an inundation depth estimation algorithm (Bryant et al., 2022), to obtain total inundation levels for Mozambique (Figure 3a). The difference between factual and counterfactual flooding is illustrated in the densely populated area of Beira (Figure 3b), the city where TC Idai made landfall and destroyed 90% of all houses according to some disaster reports (ReliefWeb, 2019). Differences in both flood extent and depth are observable between the factual (Figure 3c) and counterfactual scenario (Figure 3d). Notably, in a world without climate change, the area inundated by 100 cm or more is dramatically reduced.

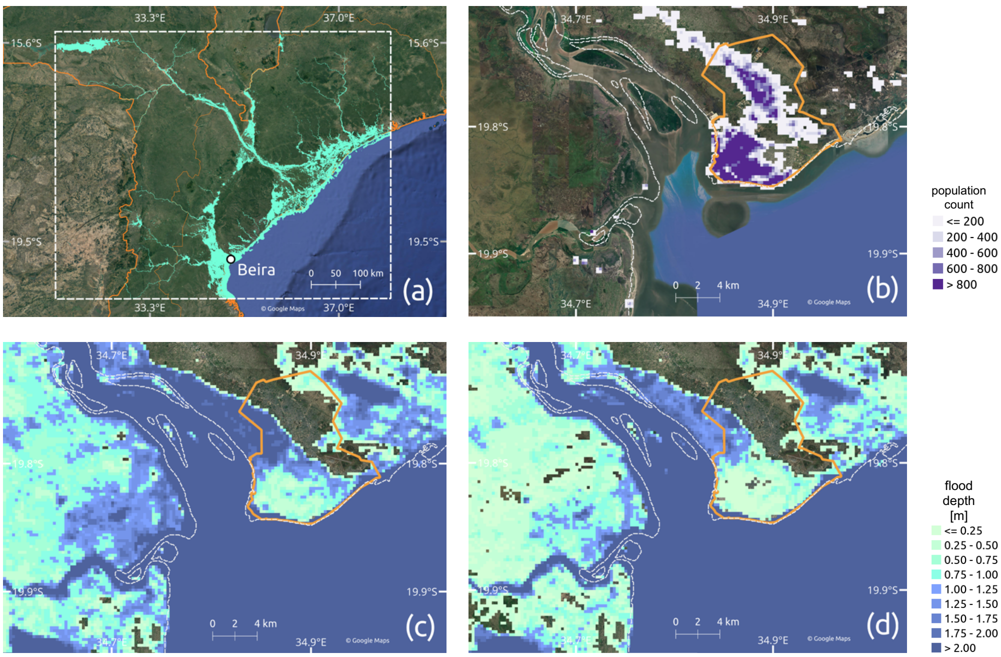

Figure 3: Simulated flood extent for Mozambique; population distribution and inundation levels for the greater area of Beira. (a) Combined factual estimate of inland and coastal flooding (binary; flood/no-flood). White dashed box shows the area of interest in which flood exposure is computed. (b) Population distribution for the greater area of Beira. Flood extent and levels for (c) the factual scenario, and (d) the "counterfactual TC intensity + sea level rise (10.5 cm)" scenario. City neighborhoods of Beira (HDX, 2019) are indicated by orange lines and shoreline (Wessel and Smith, 1996) is represented by dashed white lines in (b), (c), and (d); satellite image background by © Google Maps (Google Maps (b), 2022).

3.3 Displacement

In the next step, we investigate how the factual and counterfactual flood estimates translate into population at risk of displacement for the whole of Mozambique. Our analysis shows that the intensification of TC wind speeds leads to an increase in flood affected people and, consequently, in displacements by up to 3.6%, while counterfactuals regarding the sea level lead to only small changes (Figure 4). A combination of both counterfactuals only slightly exceeds the range as in contrast when considering the TC de-intensification alone. Despite the large uncertainty regarding SLR since 1900, the difference in the number of people affected (or displaced) is rather marginal; being less than 1% between the largest and the smallest SLR estimate. Our results highlight that the tide assumption plays a major role. The minimum and mean tide lead to marginal changes in affected/displaced people, in contrast to the maximum astronomical tide and monthly mean sea level from satellite altimetry, which show a median change in 3.1% and 3.5%, respectively. Given the high number of affected people, already small changes in the counterfactual scenarios lead to high changes in absolute numbers. The coupled effect of higher wind speeds and higher sea level increases the number of affected people and displacements by up to 43,300 and 16,500 (maximum tide) and 44,300 and 17,100 (monthly mean), respectively. Results regarding impact flood levels of 10 cm and 50 cm are displayed in the supplementary material (Figure S5 and S6), showing even higher changes for the counterfactual scenarios of up to 69,800 displacements (17.1%).

We assume that high wind speed caused only a marginal fraction of displacements, following disaster reports, media coverage and experience from other events; as an extreme example, wind by Hurricane Sandy caused less than 0.01% of the overall damage (Strauss et al., 2021). Nonetheless, in an additional sensitivity analysis, we also account for the number of people affected by high TC wind speeds of 50 m s^{-1} or above (Sect. Methods). Our analysis reveals that the number of people affected not by flooding (maximum tide assumption, 100 cm impact threshold) but by high wind speeds ranges between 354,400 to 357,400 in the factual simulation. In the counterfactual, even the maximum wind speed attained in any grid cell outside the flooded area drops from 51.5 m s^{-1} to 46.3 m s^{-1}, i.e. below the above-mentioned threshold; thus, no people are counted as affected. If the displacement vulnerability factor to high wind speed had been the same as to flooding, then the counterfactual would imply 109,200 to 111,500 displacements, or 22.8 to 23.3% of the total displacement, attributable to climate change.

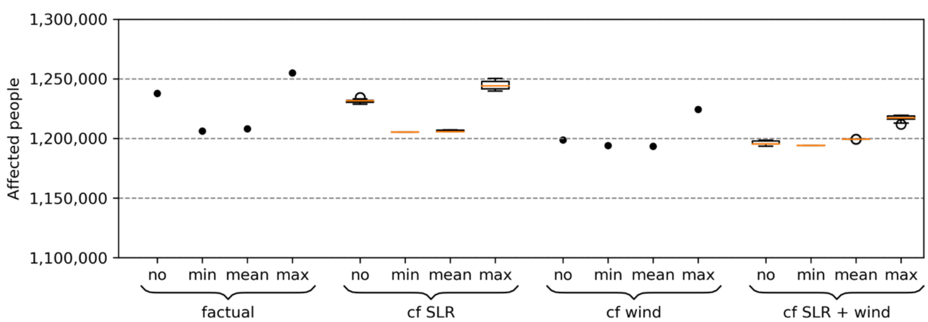

https://doi.org/10.5194/egusphere-2022-1308
Preprint. Discussion started: 9 January 2023
© Author(s) 2023. CC BY 4.0 License.

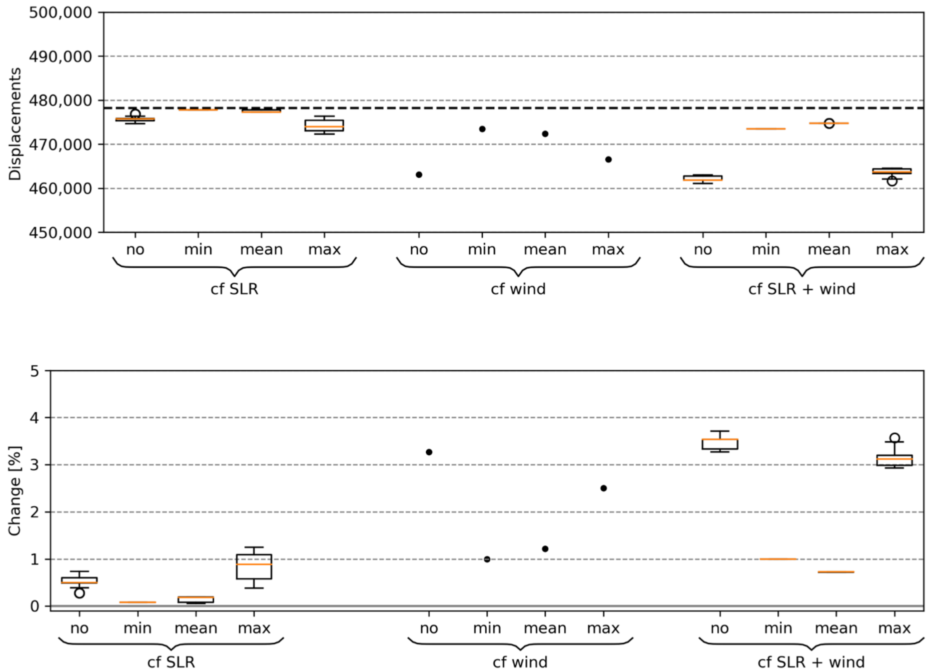

Figure 4: Simulated affected people (top), displacements (middle) and percentile change (bottom) for the 100 cm impact threshold. Three counterfactual scenarios are shown: lower sea level ("cf SLR")), de-intensification ("cf wind"), and a combination of both ("cf SLR + wind"). Additionally, a variety of counterfactual sea levels as well as a set of astronomical tides is presented, covering minimum ("min"), mean ("mean"), and maximum ("max") as well as monthly mean sea level from satellite altimetry ("no"). Bold dashed line in the middle panel shows the number of observed displacements. Percentile changes in affected people and displacements are the same. The second quartile Q2 (median) of the box plot is shown in orange, "whiskers" are placed at ±1.5 * interquartile range (Q3-Q1).

4 Discussion and conclusions

With more than one degree of global warming, most, if not all, extreme weather events now can be assumed to bear some imprint of climate change. By extension, this is also true for the humanitarian crises induced by catastrophic storms, floods, or droughts. However, while economic damages from climate change have been attributed both in case studies and global studies (Frame et al., 2020b, 2020a; Sauer et al., 2021; Strauss et al., 2021), little is known about the extent to which climate change has already exacerbated human displacement. Our modeling study of TC Idai suggests that climate change may have induced about 17,000 additional displacements from this one event. This is primarily due to the intensification of TC wind speed inducing a more powerful storm surge; and to a lesser extent due to sea level rise providing a higher baseline for the storm surge.

https://doi.org/10.5194/egusphere-2022-1308
Preprint. Discussion started: 9 January 2023
© Author(s) 2023. CC BY 4.0 License.

Our results likely underestimate the full contribution of climate change to displacement associated with TC Idai, because we solely addressed the effect of climate change on coastal flooding, neglecting changes in inland flooding. Between March 3 and 17, heavy precipitation between 200-400 mm was registered for Beira City and the region, with upstream sections of the Pungwe river basin exposed to more than 600 mm (Probst and Annunziato, 2019). With growing evidence that climate change not only affects precipitation intensity (Fowler et al., 2021; Guerreiro et al., 2018; Scherrer et al., 2016) but also continental-scale changes in fluvial flood discharge (Blöschl et al., 2019; Gudmundsson et al., 2021), it is likely that in a world without climate change, the river flood magnitude would have been smaller, and even less people would have been exposed than in our coastal-only counterfactual. Quantifying this additional effect would require a river flood model capable of reproducing the observed flood extent and associated inundation depths, and ideally coupled with a coastal flood model to capture the interaction between river flood and storm surge. Even though globally-applicable frameworks for compound flood hazard modeling are under construction, and have recently been tested for TC Idai (Eilander et al., 2022), evaluations of fluvial flood models reveal important shortcomings in data-scarce regions such as Mozambique (Bernhofen et al., 2018; Mester et al., 2021). Quantifying the role of river flooding in TC-induced displacement thus is a timely challenge.

Our main analysis also assumed no direct effect of high wind speeds on displacement, lacking clear evidence for substantial displacement due to high winds alone. Our additional sensitivity analysis suggests that changing this assumption could increase the number of displacements attributable to climate change considerably. Given this potentially large effect, and our limited understanding of the relative roles of different drivers of displacement in general, the specific vulnerability to displacement from different types of hazard should be the subject of future studies. Moreover, assuming that displacement can occur already at inundation depths of less than 100 cm also leads to higher estimates of climate change-attributable displacement, according to our sensitivity analysis. Again, a better understanding of vulnerability beyond hard thresholds will be critical to refine risk assessments.

We did not change storm track or size in our counterfactual simulations. While storm tracks may be affected by climate change (Knutson et al., 2019), we assume that Beira has not become more or less likely as a landfall site. Mean storm size is found to increase systematically with the relative sea surface temperature (Chavas et al., 2016), although numerical simulations suggest that projected median sizes remain nearly constant globally (Knutson et al., 2015). Assuming increases in storm size due to climate change would again result in higher estimates of attributable displacements in our analysis. Furthermore, uncertainties regarding the population and observatory data, such as the satellite imagery, as well as the underlying digital elevation model (DEM), used for both the inland flood depth estimation and the coastal flood model, should not be neglected (Hawker et al., 2018).

By design, in our attribution study, we assumed a fixed population distribution in both factual and counterfactual simulations, as well as a fixed, empirically determined displacement vulnerability factor, and only investigated changes in displacement risk following from changes in the physical characteristics of TC Idai and its impacts. Assessments of future risks - or of past impacts - should not only take into account the intensification of physical hazards, but also increases in exposure (Kam et al., 2021); as well as potential changes in vulnerability due to social, economic, or technological developments. Changes in vulnerability have been

https://doi.org/10.5194/egusphere-2022-1308
Preprint. Discussion started: 9 January 2023
© Author(s) 2023. CC BY 4.0 License.

studied with respect to economic damages and fatalities (Jongman et al., 2015; Sauer et al., 2021), but not for displacement.

Here, we have chosen a storyline approach for the impact attribution instead of a more traditional probabilistic attribution approach (Philip et al., 2020; Titley et al., 2016), as for instance previously employed to attribute heavy precipitation of Hurricane Harvey (Oldenborgh et al., 2017) to climate change. One reason is that for Mozambique neither the complete time series of rainfall nor the high station density required by a probabilistic approach (van Oldenborgh et al., 2021) are available. Reanalysis products for precipitation could be used as an alternative, however, their quality depends on geographic location, so the use of multiple reanalysis and/or observation products is recommended (Angélil et al., 2016). Further, in contrast to the probabilistic approach, the storyline approach allows us to investigate the driving factors involved, as well as their plausibility (Shepherd et al., 2018). Finally, framing the risk of tropical cyclones in the context of climate change in an extreme event-oriented rather than a probabilistic manner allows us to assign absolute numbers of attributable displacements, which raises risk awareness in a more tangible way.

Our study expands the scope of extreme event impact attribution to include displacement as a societal impact dimension. In general, due to the lack of calibrated regional models and gauge stations, only few attribution studies (Luu et al., 2021; Takayabu et al., 2015) focus on storms - or any extreme weather events, for that matter - in low-income countries. This not only limits our understanding of climate change effects on extreme events from a global perspective, but also biases geographically the amount of knowledge and information available to inform risk management and adaptation strategies (Otto et al., 2020). Mozambique, like many countries, is exposed not only to TCs but also other climate-related hazards, such as droughts, and at the same time facing socio-economic challenges, making it all the more important to understand and anticipate risks in a changing climate.

Code availability

The source code for this study is available from https://github.com/BenediktMester/TC_Idai_attribution.

Data availability

Satellite imagery is used with the permission of Atmospheric and Environmental Research & African Risk Capacity. Output of the flood depth algorithm, GeoClaw results, and TC Idai wind speed files can be accessed at https://zenodo.org/record/6907855 (Mester et al., 2022). GHS gridded population data is available at https://data.jrc.ec.europa.eu/dataset/jrc-ghsl-ghs_pop_gpw4_globe_r2015a#dataaccess.
National borders of Mozambique were obtained from https://gadm.org/data.html. For the trendline analysis of annual means of maximum wind speeds we use IBTraCS Version 4 database, accessible at https://www.ncei.noaa.gov/data/international-best-track-archive-for-climate-stewardship-ibtracs/v04r00/access/netcdf/IBTrACS.ALL.v04r00.nc.

https://doi.org/10.5194/egusphere-2022-1308
Preprint. Discussion started: 9 January 2023
© Author(s) 2023. CC BY 4.0 License.

All data used for the figures are publicly available. Maps were generated with QGIS, which can be downloaded at https://www.qgis.org/. Satellite imagery background by © Google Maps can be accessed via http://mt0.google.com/vt/lyrs=s&hl=en&x={x}&y={y}&z={z}. We used IBTrACS Version 4 to extract the trajectory data of tropical cyclone Idai, availabe at https://www.ncei.noaa.gov/products/international-best-track-archive?name=ib-v4-access. Mozambique admin level 4 shapefiles for Beira are available at https://data.humdata.org/dataset/mozambique-admin-level-4-beira-and-dondo-neighbourhood-boundaries. GSHHG shoreline data can be accessed via https://www.ngdc.noaa.gov/mgg/shorelines/data/gshhg/latest/.

Author contributions

B.M. and J.S. designed the study, with contributions from T.V., C.O., and K.F. T.V. designed and performed coastal flood model calculations. S.B. estimated flood depths from satellite imagery. B.M. computed the number of affected people and displacements. B.M. and J.S. analyzed the results, and C.O., and K.F. contributed to the interpretation. B.M., T.V., S.B., C.O. and J.S. jointly wrote the paper.

Competing interests

The authors declare no competing interests.

Acknowledgments

This research received funding from the European Union's Horizon 2020 research and innovation programme under grant agreement No 820712 (RECEIPT).

References

Angélil, O., Perkins-Kirkpatrick, S., Alexander, L.V., Stone, D., Donat, M.G., Wehner, M., Shiogama, H., Ciavarella, A., Christidis, N., 2016. Comparing regional precipitation and temperature extremes in climate model and reanalysis products. Weather Clim. Extrem. 13, 35–43. https://doi.org/10.1016/j.wace.2016.07.001

Atmospheric and Environmental Research & African Risk Capacity, 2022. Flood depictions: AER AFED v05r01.

Beal, L.M., Vialard, J., Roxy, M.K., lead authors, 2019. IndOOS-2: A roadmap to sustained observations of the Indian Ocean for 2020-203 CLIVAR-4/2019, GOOS-237, 206 pp., 218.

Bernhofen, M.V., Whyman, C., Trigg, M.A., Sleigh, P.A., Smith, A.M., Sampson, C.C., Yamazaki, D., Ward, P.J., Rudari, R., Pappenberger, F., Dottori, F., Salamon, P., Winsemius, H.C., 2018. A first collective validation of global fluvial flood models for major floods in Nigeria and Mozambique. Environ. Res. Lett. 13, 104007. https://doi.org/10.1088/1748-9326/aae014

Blöschl, G., Hall, J., Viglione, A., Perdigão, R.A.P., Parajka, J., Merz, B., Lun, D., Arheimer, B., Aronica, G.T., Bilibashi, A., Boháč, M., Bonacci, O., Borga, M., Čanjevac, I., Castellarin, A., Chirico, G.B., Claps, P., Frolova, N., Ganora, D., Gorbachova, L., Gül,

https://doi.org/10.5194/egusphere-2022-1308
Preprint. Discussion started: 9 January 2023
© Author(s) 2023. CC BY 4.0 License.

A., Hannaford, J., Harrigan, S., Kireeva, M., Kiss, A., Kjeldsen, T.R., Kohnová, S., Koskela, J.J., Ledvinka, O., Macdonald, N., Mavrova-Guirguinova, M., Mediero, L., Merz, R., Molnar, P., Montanari, A., Murphy, C., Osuch, M., Ovcharuk, V., Radevski, I., Salinas, J.L., Sauquet, E., Šraj, M., Szolgay, J., Volpi, E., Wilson, D., Zaimi, K., Živković, N., 2019. Changing climate both increases and decreases European river floods. Nature 573, 108–111. https://doi.org/10.1038/s41586-019-1495-6

Bryant, S., McGrath, H., Boudreault, M., 2022. Gridded flood depth estimates from satellite-derived inundations. Nat. Hazards Earth Syst. Sci. 22, 1437–1450. https://doi.org/10.5194/nhess-22-1437-2022

Chavas, D.R., Lin, N., Dong, W., Lin, Y., 2016. Observed Tropical Cyclone Size Revisited. J. Clim. 29, 2923–2939. https://doi.org/10.1175/JCLI-D-15-0731.1

Church, J.A., Clark, P.U., Cazenave, A., Gregory, J.M., Jevrejeva, S., Levermann, A., Merrifield, M.A., Milne, G.A., Nerem, R.S., Nunn, P.D., Payne, A.J., Pfeffer, W.T., Stammer, D., Unnikrishnan, A.S., 2013. Sea Level Change. In: Climate Change 2013: The Physical Science Basis. Contribution of Working Group I to the Fifth Assessment Report of the Intergovernmental Panel on Climate Change [Stocker, T.F., D. Qin, G.-K. Plattner, M. Tignor, S.K. Allen, J. Boschung, A. Nauels, Y. Xia, V. Bex and P.M. Midgley (eds.)]. Cambridge University Press, Cambridge, United Kingdom and New York, NY, USA, pp. 1137–1216.

Church, J.A., White, N.J., 2011. Sea-Level Rise from the Late 19th to the Early 21st Century. Surv. Geophys. 32, 585–602. https://doi.org/10.1007/s10712-011-9119-1

Church, J.A., White, N.J., Coleman, R., Lambeck, K., Mitrovica, J.X., 2004. Estimates of the Regional Distribution of Sea Level Rise over the 1950–2000 Period. J. Clim. 17, 2609–2625. https://doi.org/10.1175/1520-0442(2004)017<2609:EOTRDO>2.0.CO;2

CMEMS, 2021. Global ocean gridded L4 sea surface heights and derived variables reprocessed (1993-ongoing). E.U. Copernicus Marine Service (CMEMS). Downloaded 2021-08-02.

Cohen, S., Brakenridge, G.R., Kettner, A., Bates, B., Nelson, J., McDonald, R., Huang, Y.-F., Munasinghe, D., Zhang, J., 2018. Estimating Floodwater Depths from Flood Inundation Maps and Topography. JAWRA J. Am. Water Resour. Assoc. 54, 847–858. https://doi.org/10.1111/1752-1688.12609

Custer, R., Nishijima, K., 2015. Flood vulnerability assessment of residential buildings by explicit damage process modelling. Nat. Hazards 78, 461–496. https://doi.org/10.1007/s11069-015-1725-7

Dangendorf Sönke, Marcos Marta, Wöppelmann Guy, Conrad Clinton P., Frederikse Thomas, Riva Riccardo, 2017. Reassessment of 20th century global mean sea level rise. Proc. Natl. Acad. Sci. 114, 5946–5951. https://doi.org/10.1073/pnas.1616007114

Desai, B., Bresch, D.N., Cazabat, C., Hochrainer-Stigler, S., Mechler, R., Ponserre, S., Schewe, J., 2021. Addressing the human cost in a changing climate. Science 372, 1284–1287. https://doi.org/10.1126/science.abh4283

Dullaart, J.C.M., Muis, S., Bloemendaal, N., Chertova, M.V., Couasnon, A., Aerts, J.C.J.H., 2021. Accounting for tropical cyclones more than doubles the global population exposed to low-probability coastal flooding. Commun. Earth Environ. 2, 135. https://doi.org/10.1038/s43247-021-00204-9

Eilander, D., Couasnon, A., Leijnse, T., Ikeuchi, H., Yamazaki, D., Muis, S., Dullaart, J., Winsemius, H.C., Ward, P.J., 2022. A globally-applicable framework for compound flood hazard modeling. EGUsphere 2022, 1–40. https://doi.org/10.5194/egusphere-2022-149

Emanuel, K.A., 1987. The dependence of hurricane intensity on climate. Nature 326, 483–485. https://doi.org/10.1038/326483a0

Fowler, H.J., Lenderink, G., Prein, A.F., Westra, S., Allan, R.P., Ban, N., Barbero, R., Berg, P., Blenkinsop, S., Do, H.X., Guerreiro, S., Haerter, J.O., Kendon, E.J., Lewis, E., Schaer, C., Sharma, A., Villarini, G., Wasko, C., Zhang, X., 2021. Anthropogenic intensification of short-duration rainfall extremes. Nat. Rev. Earth Environ. 2, 107–

https://doi.org/10.5194/egusphere-2022-1308
Preprint. Discussion started: 9 January 2023
© Author(s) 2023. CC BY 4.0 License.

122. https://doi.org/10.1038/s43017-020-00128-6

Fox-Kemper, B., Hewitt, H.T., Xiao, C., Aðalgeirsdóttir, G., Drijfhout, S.S., Edwards, T.L., Golledge, N.R., Hemer, M., Kopp, R.E., Krinner, G., Mix, A., Notz, D., Nowicki, S., Nurhati, I.S., Ruiz, L., Sallée, J.-B., Slangen, A.B.A., Yu, Y., 2021. Ocean, Cryosphere and Sea Level Change. In Climate Change 2021: The Physical Science Basis. Contribution of Working Group I to the Sixth Assessment Report of the Intergovernmental Panel on Climate Change [Masson-Delmotte, V., P. Zhai, A. Pirani, S.L. Connors, C. Péan, S. Berger, N. Caud, Y. Chen, L. Goldfarb, M.I. Gomis, M. Huang, K. Leitzell, E. Lonnoy, J.B.R. Matthews, T.K. Maycock, T. Waterfield, O. Yelekçi, R. Yu, and B. Zhou (eds.)]. Cambridge University Press, Cambridge, United Kingdom and New York, NY, USA, pp. 1211–1362.

Frame, D.J., Rosier, S.M., Noy, I., Harrington, L.J., Carey-Smith, T., Sparrow, S.N., Stone, D.A., Dean, S.M., 2020a. Climate change attribution and the economic costs of extreme weather events: a study on damages from extreme rainfall and drought. Clim. Change 162, 781–797. https://doi.org/10.1007/s10584-020-02729-y

Frame, D.J., Wehner, M.F., Noy, I., Rosier, S.M., 2020b. The economic costs of Hurricane Harvey attributable to climate change. Clim. Change 160, 271–281. https://doi.org/10.1007/s10584-020-02692-8

GADM, 2018. Database of Global Administrative Areas.

Galantowicz, J.F., Picton, J., 2021. Flood Mapping with Passive Microwave Remote Sensing: Current Capabilities and Directions for Future Development, in: Earth Observation for Flood Applications. Elsevier, p. 28.

Garner Andra J., Mann Michael E., Emanuel Kerry A., Kopp Robert E., Lin Ning, Alley Richard B., Horton Benjamin P., DeConto Robert M., Donnelly Jeffrey P., Pollard David, 2017. Impact of climate change on New York City's coastal flood hazard: Increasing flood heights from the preindustrial to 2300 CE. Proc. Natl. Acad. Sci. 114, 11861–11866. https://doi.org/10.1073/pnas.1703568114

Geiger, T., Frieler, K., Bresch, D.N., 2018. A global historical data set of tropical cyclone exposure (TCE-DAT). Earth Syst. Sci. Data 10, 185–194. https://doi.org/10.5194/essd-10-185-2018

Google Maps (a), 2022. Mozambique. Satellite image. URL: http://mt0.google.com/vt/lyrs=s&hl=en&x={x}&y={y}&z={z}. Accessed on 2022-04-27.

Google Maps (b), 2022. Greater Area of Beira, Mozambique. Satellite image. URL: http://mt0.google.com/vt/lyrs=s&hl=en&x={x}&y={y}&z={z}. Accessed on 2022-04-27.

Gudmundsson, L., Boulange, J., Do, H.X., Gosling, S.N., Grillakis, M.G., Koutroulis, A.G., Leonard, M., Liu, J., Müller Schmied, H., Papadimitriou, L., Pokhrel, Y., Seneviratne, S.I., Satoh, Y., Thiery, W., Westra, S., Zhang, X., Zhao, F., 2021. Globally observed trends in mean and extreme river flow attributed to climate change. Science 371, 1159–1162. https://doi.org/10.1126/science.aba3996

Guerreiro, S.B., Fowler, H.J., Barbero, R., Westra, S., Lenderink, G., Blenkinsop, S., Lewis, E., Li, X.-F., 2018. Detection of continental-scale intensification of hourly rainfall extremes. Nat. Clim. Change 8, 803–807. https://doi.org/10.1038/s41558-018-0245-3

Guha-Sapir, D., Below, R., Hoyois, P., 2022. EM-DAT: The CRED/OFDA International Disaster Database. Université Catholique de Louvain-Brussels, Belgium.

Gulev, S.K., Thorne, P.W., Ahn, J., Dentener, F.J., Domingues, C.M., Gerland, S., Gong, D., Kaufman, D.S., Nnamchi, H.C., Quaas, J., Rivera, J.A., Sathyendranath, S., Smith, S.L., Trewin, B., von Schuckmann, K., Vose, R.S., 2021. Changing State of the Climate System. In Climate Change 2021: The Physical Science Basis. Contribution of Working Group I to the Sixth Assessment Report of the Intergovernmental Panel on Climate Change [Masson-Delmotte, V., P. Zhai, A. Pirani, S.L. Connors, C. Péan, S. Berger, N. Caud, Y. Chen, L. Goldfarb, M.I. Gomis, M. Huang, K. Leitzell, E. Lonnoy, J.B.R. Matthews, T.K. Maycock, T. Waterfield, O. Yelekçi, R. Yu, and B. Zhou (eds.)]. Cambridge University Press. In Press.

Han, W., Meehl, G.A., Rajagopalan, B., Fasullo, J.T., Hu, A., Lin, J., Large, W.G., Wang, J., Quan, X.-W., Trenary, L.L., Wallcraft, A., Shinoda, T., Yeager, S., 2010. Patterns of

https://doi.org/10.5194/egusphere-2022-1308
Preprint. Discussion started: 9 January 2023
© Author(s) 2023. CC BY 4.0 License.

Indian Ocean sea-level change in a warming climate. Nat. Geosci. 3, 546–550. https://doi.org/10.1038/ngeo901

Hawker, L., Rougier, J., Neal, J., Bates, P., Archer, L., Yamazaki, D., 2018. Implications of Simulating Global Digital Elevation Models for Flood Inundation Studies. Water Resour. Res. 54, 7910–7928. https://doi.org/10.1029/2018WR023279

HDX, 2019. Mozambique admin level 4 - Beira and Dondo neighbourhood boundaries.

Holland, G.J., 1980. An Analytic Model of the Wind and Pressure Profiles in Hurricanes. Mon. Weather Rev. 108, 1212–1218. https://doi.org/10.1175/1520-0493(1980)108<1212:AAMOTW>2.0.CO;2

IDMC, 2022. “IDMC Global Report on Internal Displacement 2022 Displacement Dataset.” https://www.internal-displacement.org/database/displacement-data.

Irish, J.L., Sleath, A., Cialone, M.A., Knutson, T.R., Jensen, R.E., 2014. Simulations of Hurricane Katrina (2005) under sea level and climate conditions for 1900. Clim. Change 122, 635–649. https://doi.org/10.1007/s10584-013-1011-1

Jongman, B., Winsemius, H.C., Aerts, J.C.J.H., Coughlan de Perez, E., van Aalst, M.K., Kron, W., Ward, P.J., 2015. Declining vulnerability to river floods and the global benefits of adaptation. Proc. Natl. Acad. Sci. 112, E2271–E2280. https://doi.org/10.1073/pnas.1414439112

Kam, P.M., Aznar-Siguan, G., Schewe, J., Milano, L., Ginnetti, J., Willner, S., McCaughey, J.W., Bresch, D.N., 2021. Global warming and population change both heighten future risk of human displacement due to river floods. Environ. Res. Lett. 16, 044026. https://doi.org/10.1088/1748-9326/abd26c

Knapp, K.R., Kruk, M.C., Levinson, D.H., Diamond, H.J., Neumann, C.J., 2010. The International Best Track Archive for Climate Stewardship (IBTrACS): Unifying Tropical Cyclone Data. Bulletin of the American Meteorological Society 91 (3): 363-76.

Knutson, T., Camargo, S.J., Chan, J.C.L., Emanuel, K., Ho, C.-H., Kossin, J., Mohapatra, M., Satoh, M., Sugi, M., Walsh, K., Wu, L., 2020. Tropical Cyclones and Climate Change Assessment: Part II: Projected Response to Anthropogenic Warming. Bull. Am. Meteorol. Soc. 101, E303–E322. https://doi.org/10.1175/BAMS-D-18-0194.1

Knutson, T., Camargo, S.J., Chan, J.C.L., Emanuel, K., Ho, C.-H., Kossin, J., Mohapatra, M., Satoh, M., Sugi, M., Walsh, K., Wu, L., 2019. Tropical Cyclones and Climate Change Assessment: Part I: Detection and Attribution. Bull. Am. Meteorol. Soc. 100, 1987–2007. https://doi.org/10.1175/BAMS-D-18-0189.1

Knutson, T.R., Sirutis, J.J., Zhao, M., Tuleya, R.E., Bender, M., Vecchi, G.A., Villarini, G., Chavas, D., 2015. Global Projections of Intense Tropical Cyclone Activity for the Late Twenty-First Century from Dynamical Downscaling of CMIP5/RCP4.5 Scenarios. J. Clim. 28, 7203–7224. https://doi.org/10.1175/JCLI-D-15-0129.1

Knutson, T.R., Tuleya, R.E., 2008. Tropical cyclones and climate change: revisiting recent studies at GFDL, in: Diaz, H.F., Murnane, R.J. (Eds.), Climate Extremes and Society. Cambridge University Press, Cambridge, pp. 120–144. https://doi.org/10.1017/CBO9780511535840.010

Kossin, J.P., Olander, T.L., Knapp, K.R., 2013. Trend Analysis with a New Global Record of Tropical Cyclone Intensity. J. Clim. 26, 9960–9976. https://doi.org/10.1175/JCLI-D-13-00262.1

Kulp, S.A., Strauss, B.H., 2021. CoastalDEM v2.1: A high-accuracy and high-resolution global coastal elevation model trained on ICESat-2 satellite lidar. Climate Central Scientific Report 17.

Kulp, S.A., Strauss, B.H., 2018. CoastalDEM: A global coastal digital elevation model improved from SRTM using a neural network. Remote Sens. Environ. 206, 231–239. https://doi.org/10.1016/j.rse.2017.12.026

Lin, N., Emanuel, K., Oppenheimer, M., Vanmarcke, E., 2012. Physically based assessment of hurricane surge threat under climate change. Nat. Clim. Change 2, 462–467. https://doi.org/10.1038/nclimate1389

Luu, L.N., Scussolini, P., Kew, S., Philip, S., Hariadi, M.H., Vautard, R., Van Mai, K., Van Vu,

https://doi.org/10.5194/egusphere-2022-1308
Preprint. Discussion started: 9 January 2023
© Author(s) 2023. CC BY 4.0 License.

T., Truong, K.B., Otto, F., van der Schrier, G., van Aalst, M.K., van Oldenborgh, G.J., 2021. Attribution of typhoon-induced torrential precipitation in Central Vietnam, October 2020. Clim. Change 169, 24. https://doi.org/10.1007/s10584-021-03261-3

Lyard, F.H., Allain, D.J., Cancet, M., Carrère, L., Picot, N., 2021. FES2014 global ocean tide atlas: design and performance. Ocean Sci. 17, 615–649. https://doi.org/10.5194/os-17-615-2021

Mandli, K.T., Dawson, C.N., 2014. Adaptive mesh refinement for storm surge. Ocean Model. 75, 36–50. https://doi.org/10.1016/j.ocemod.2014.01.002

Mester, B., Vogt, T., Bryant, S., Otto, C., Frieler, K., Schewe, J., 2022. TC Idai attribution study - data collection v1.1 (Version v1.1). doi: 10.5281/zenodo.6907855.

Mester, B., Willner, S.N., Frieler, K., Schewe, J., 2021. Evaluation of river flood extent simulated with multiple global hydrological models and climate forcings. Environ. Res. Lett. 16, 094010. https://doi.org/10.1088/1748-9326/ac188d

Muis, S., Apecechea, M.I., Dullaart, J., de Lima Rego, J., Madsen, K.S., Su, J., Yan, K., Verlaan, M., 2020. A High-Resolution Global Dataset of Extreme Sea Levels, Tides, and Storm Surges, Including Future Projections. Front. Mar. Sci. 7. https://doi.org/10.3389/fmars.2020.00263

Nicholls, R.J., Lincke, D., Hinkel, J., Brown, S., Vafeidis, A.T., Meyssignac, B., Hanson, S.E., Merkens, J.-L., Fang, J., 2021. A global analysis of subsidence, relative sea-level change and coastal flood exposure. Nat. Clim. Change 11, 338–342. https://doi.org/10.1038/s41558-021-00993-z

Oldenborgh, G.J. van, Wiel, K. van der, Sebastian, A., Singh, R., Arrighi, J., Otto, F., Haustein, K., Li, S., Vecchi, G., Cullen, H., 2017. Attribution of extreme rainfall from Hurricane Harvey, August 2017. Environ. Res. Lett. 12, 124009. https://doi.org/10.1088/1748-9326/aa9ef2

O'Neill, B., van Aalst, M., Zaiton Ibrahim, Z., Berrang Ford, L., Bhadwal, S., Buhaug, H., Diaz, D., Frieler, K., Garschagen, M., Magnan, A., Midgley, G., Mirzabaev, A., Thomas, A., Warren, R., 2022. Key Risks Across Sectors and Regions. In: Climate Change 2022: Impacts, Adaptation, and Vulnerability. Contribution of Working Group II to the Sixth Assessment Report of the Intergovernmental Panel on Climate Change [H.-O. Pörtner, D.C. Roberts, M. Tignor, E.S. Poloczanska, K. Mintenbeck, A. Alegría, M. Craig, S. Langsdorf, S. Löschke, V. Möller, A. Okem, B. Rama (eds.)]. Cambridge University Press.

Otto, F.E.L., Harrington, L., Schmitt, K., Philip, S., Kew, S., Oldenborgh, G.J. van, Singh, R., Kimutai, J., Wolski, P., 2020. Challenges to Understanding Extreme Weather Changes in Lower Income Countries. Bull. Am. Meteorol. Soc. 101, E1851–E1860. https://doi.org/10.1175/BAMS-D-19-0317.1

Pekel, J.-F., Cottam, A., Gorelick, N., Belward, A.S., 2016. High-resolution mapping of global surface water and its long-term changes. Nature 540, 418–422. https://doi.org/10.1038/nature20584

Probst, P., Annunziato, A., 2019. Tropical Cyclone IDAI: analysis of the wind, rainfall and storm surge impact. Join Research Centre (EUROPEAN COMMISSION).

Reliefweb, 2019. Mozambique: Cyclone Idai & Floods Flash Update No. 10, 26 March 2019. URL: https://reliefweb.int/report/mozambique/southern-africa-cyclone-idai-snapshot-26-march- 2019. Accessed on 2021-10-29.

ReliefWeb, 2019. 'The First City Completely Devastated by Climate Change' Tries to Rebuild after Cyclone Idai.

Resio, D.T., Irish, J.L., 2016. Tropical Cyclone Storm Surge Risk, in: Handbook of Coastal and Ocean Engineering. WORLD SCIENTIFIC, pp. 1405–1422. https://doi.org/10.1142/9789813204027_0049

Sauer, I.J., Reese, R., Otto, C., Geiger, T., Willner, S.N., Guillod, B.P., Bresch, D.N., Frieler, K., 2021. Climate signals in river flood damages emerge under sound regional disaggregation. Nat. Commun. 12, 2128. https://doi.org/10.1038/s41467-021-22153-9

Scherrer, S.C., Fischer, E.M., Posselt, R., Liniger, M.A., Croci-Maspoli, M., Knutti, R., 2016.

© Author(s) 2023. CC BY 4.0 License.

Emerging trends in heavy precipitation and hot temperature extremes in Switzerland. J. Geophys. Res. Atmospheres 121, 2626–2637. https://doi.org/10.1002/2015JD024634
Schiavina, M., Freire, S., MacManus, K., 2019. GHS population grid multitemporal (1975, 1990, 2000, 2015) R2019A. European Commission, Joint Research Centre (JRC). https://doi.org/10.2905/42E8BE89-54FF-464E-BE7B-BF9E64DA5218
Shepherd, T.G., 2016. A Common Framework for Approaches to Extreme Event Attribution. Curr. Clim. Change Rep. 2, 28–38. https://doi.org/10.1007/s40641-016-0033-y
Shepherd, T.G., Boyd, E., Calel, R.A., Chapman, S.C., Dessai, S., Dima-West, I.M., Fowler, H.J., James, R., Maraun, D., Martius, O., Senior, C.A., Sobel, A.H., Stainforth, D.A., Tett, S.F.B., Trenberth, K.E., van den Hurk, B.J.J.M., Watkins, N.W., Wilby, R.L., Zenghelis, D.A., 2018. Storylines: an alternative approach to representing uncertainty in physical aspects of climate change. Clim. Change 151, 555–571. https://doi.org/10.1007/s10584-018-2317-9
Strauss, B.H., Orton, P.M., Bittermann, K., Buchanan, M.K., Gilford, D.M., Kopp, R.E., Kulp, S., Massey, C., Moel, H. de, Vinogradov, S., 2021. Economic damages from Hurricane Sandy attributable to sea level rise caused by anthropogenic climate change. Nat. Commun. 12, 2720. https://doi.org/10.1038/s41467-021-22838-1
Takayabu, I., Hibino, K., Sasaki, H., Shiogama, H., Mori, N., Shibutani, Y., Takemi, T., 2015. Climate change effects on the worst-case storm surge: a case study of Typhoon Haiyan. Environ. Res. Lett. 10, 064011. https://doi.org/10.1088/1748-9326/10/6/064011
The World Bank, 2022. World Development Indicators. Population, total - Mozambique.
Tozer, B., Sandwell, D.T., Smith, W.H.F., Olson, C., Beale, J.R., Wessel, P., 2019. Global Bathymetry and Topography at 15 Arc Sec: SRTM15+. Earth Space Sci. 6, 1847–1864. https://doi.org/10.1029/2019EA000658
van Oldenborgh, G.J., van der Wiel, K., Kew, S., Philip, S., Otto, F., Vautard, R., King, A., Lott, F., Arrighi, J., Singh, R., van Aalst, M., 2021. Pathways and pitfalls in extreme event attribution. Clim. Change 166, 13. https://doi.org/10.1007/s10584-021-03071-7
Vogt, T., Treu, S., Mengel, M., Frieler, K., Otto, C., 2022. Assessing the scope and limitations of a fully-open global TC surge model. Manuscript in preparation.
Warren, M., 2019. Why Cyclone Idai is one of the Southern Hemisphere's most devastating storms. Nature. https://doi.org/10.1038/d41586-019-00981-6
Wessel, P., Smith, W., 1996. A global, self-consistent, hierarchical, high-resolution shoreline database. J. Geophys. Res. 101, 8741–8743. https://doi.org/10.1029/96JB00104
Wulder, M.A., White, J.C., Loveland, T.R., Woodcock, C.E., Belward, A.S., Cohen, W.B., Fosnight, E.A., Shaw, J., Masek, J.G., Roy, D.P., 2016. The global Landsat archive: Status, consolidation, and direction. Remote Sens. Environ. 185, 271–283.
Yamazaki, D., Ikeshima, D., Sosa, J., Bates, P.D., Allen, G.H., Pavelsky, T.M., 2019. MERIT Hydro: A High-Resolution Global Hydrography Map Based on Latest Topography Dataset. Water Resour. Res. 55, 5053–5073. https://doi.org/10.1029/2019WR024873